Discovery of Soft Spectral Component and Transient 22.7s Quasi Periodic Oscillations of SAX J2103.5+4545

S. Ç. İnam and A. Baykal

Department of Physics, Middle East Technical University, Inonu Bulvari, Balgat, Ankara 06531 Turkey

`scinam@metu.edu.tr, altan@astroa.physics.metu.edu.tr`

J. Swank

NASA Goddard Space Flight Center, Greenbelt, MD 20771 USA

`swank@xenos.gsfc.nasa.gov`

and

M.J.Stark

Department of Physics, Lafayette College, Easton, PA 18042 USA

`starkm@lafayette.edu`

ABSTRACT

XMM-Newton observed SAX J2103.5+4545 on January 6, 2003, while RXTE was monitoring the source. Using RXTE-PCA dataset between December 3, 2002 and January 29, 2003, the spin period and average spin-up rate during the XMM-Newton observations were found to be 354.7940 ± 0.0008 s and $(7.4\pm0.9)\times10^{-13}$Hz s^{-1} respectively. In the power spectrum of the 0.9-11 keV EPIC-PN lightcurve, we found quasi periodic oscillations around 0.044 Hz (22.7 s) with an rms fractional amplitude $\sim$6.6 %. We interpreted this QPO feature as the Keplerian motion of inhomogenuities through the inner disk. In the X-ray spectrum, in addition to the power law component with high energy cutoff and $\sim$ 6.4 keV fluorescent iron emission line (Baykal et al., 2002), we discovered a soft component consistent with a blackbody emission with kT $\sim$ 1.9keV. The pulse phase spectroscopy of the source revealed that the blackbody flux peaked at the peak of the pulse with an emission radius $\sim$ 0.3 km, suggesting the polar cap on the neutron star surface as the source of blackbody emission. The flux of the iron emission line at $\sim$ 6.42 keV was shown to peak at the off-pulse phase, supporting the idea that

this feature arises from fluorescent emission of the circumstellar material around the neutron star rather than the hot region in the vicinity of the neutron star polar cap.

Subject headings: stars: individual (SAX J2103.5+4545) — stars: neutron — X-rays: binaries — X-rays: stars

1. Introduction

The transient X-ray source SAX J2103.5+4545 was discovered by the Wide Field Camera on the *BeppoSAX* X-ray observatory during its outburst between 1997 February and September with 358.61s pulsations and a spectrum consistent with an absorbed power law model with the photon index of ~ 1.27 and the absorption column density of $\sim 3.1 \times 10^{22} \text{cm}^{-2}$ (Hulleman, in't Zand, & Heise 1998).

After detection of another outburst in November 1999 by the *all-sky monitor (ASM)* on the *Rossi X-ray Timing Explorer (RXTE)*, the source was found to be active for more than a year, and was continously monitored through regular pointed *RXTE* observations. Using pulse arrival times, the orbital period and eccentricity of the orbit were found to be 12.68(25) days and 0.4(2) (Baykal, Stark, & Swank 2000a,b). In the timing analysis, the source was initially found to be spinning up for ~ 150 days, at which point the flux dropped quickly by a factor of $\simeq 7$, and a weak spin-down began afterwards (Baykal, Stark, & Swank 2002). Strong correlation between X-ray flux and spin-up rate was explained by using Ghosh & Lamb (1979) accretion disk model. The X-ray spectra well fitted the absorbed power law model with high energy cutoff and a $\sim$6.4 keV fluorescent emission line (Baykal et al. 2002).

Orbital parameters found by using *RXTE* observations of the source (Baykal et al. 2000a,2000b) indicated that the source has a high mass companion. Hullemann et al. (1998) pointed out a B8 type star within the BeppoSAX error box, but its distance (~ 0.7 kpc) implied a luminosity too low to explain the spin-up that was seen in the RXTE observations. Recently, a possible candidate for the optical companion of SAX J2103.5+4545 with the visual magnitude of 14.2 was discovered (Reig & Mavromatakis, 2003).

SAX J2103.5+4545 was also observed with the *INTEGRAL* observatory in the 3-200 keV band with significant detection up to ~ 100 keV (Lutovinov, Molkov,& Revnivtsev 2003). The spectral parameters found in the *INTEGRAL* observations of the source were found to be compatible with those found by Baykal et al. (2002).

Since the beginning of the most recent outburst in June 2002, SAX J2103.5+4545 has

been monitored continously by *RXTE* through regular pointed observations. It was possible to obtain some simultaneous coverage with the *XMM-Newton* observatory on January 6, 2003. The observation of *XMM-Newton* revealed a soft spectral component of the source which was well-represented by a blackbody model. This spectral model was verified by simultaneous fitting of January 6, 2003 *RXTE*-PCA observation. Using *XMM-Newton* dataset, we also discovered $\sim$ 22.7s quasi periodic oscillations (QPO's) of this source for the first time. In this paper, we present our spectral and timing results of the analysis of RXTE and XMM datasets of SAX J2103.5+4545.

2. Observations

2.1. RXTE

We analyzed RXTE observations of SAX J2103.5+4545 between December 3, 2002 and January 29, 2003 with a total observation time of $\sim$ 52ksec. This set of observations is a subset of the RXTE observations for the proposal number 70082. The results presented here are based on data collected with the Proportional Counter Array (PCA; Jahoda et al., 1996). The PCA instrument consists of an array of 5 proportional counters (PCU) operating in the 2-60 keV energy range, with a total effective area of approximately 6250 cm^2 and a field of view of $\sim$ 1° FWHM. Although the number of active PCU's varied between 2 and 5 during the observations, our observations belong to the observational epoch for which background level for one of the PCUs (PCU0) increased due to the fact that this PCU started to operate without a propane layer. The latest combined background models (CM) were used together with FTOOLS 5.2 to estimate the appropriate background.

2.2. XMM

XMM-Newton observations took place on January 6, 2003 with an 8.7 ksec continuous exposure. Among the three EPIC detectors (Turner et al. 2001; Strüder et al. 2001), the MOS1 and MOS2 detectors were configured in Fast Uncompressed mode, while the PN was configured in Fast Timing mode. Data collected by the EPIC detectors on *XMM-Newton* were processed using version 5.4.1 of the *XMM-Newton* Science Analysis System (SAS). We did not include the data collected by the two Reflection Grating Spectrometers (RGS1 and RGS2) in data analysis since the count rates from these spectrometers were too low.

3. Data Analysis

3.1. Pulse Timing and Pulse profiles

In the timing analysis, we corrected the background subtracted lightcurves of RXTE data to the barycenter of solar system. The data have also been corrected for the orbit model using the eccentric orbital parameters given by Baykal et al. (2000b) with the new orbital epoch being MJD 52633.90 ∓ 0.05. In order to estimate the pulse frequency and pulse frequency derivative accurately, we used ~ 57.5 days time span of RXTE observations between MJD 52611.48 and MJD 52668.90 which covers ~ 8.7 ksec short observation of XMM data starting at MJD 52645.85. We obtained the nominal pulse frequency by using Fourier transform and constructed 20 pulse profiles (one pulse profile for each RXTE orbit) by folding the lightcurve at this nominal pulse period. We found the pulse arrival times (phase offsets) by cross-correlating these pulse profiles with a template chosen as the most statistically significant pulse profile. In the pulse timing analysis, we used the harmonic representation of the pulse profiles (Deeter & Boynton 1985). In this technique, the pulse profiles are expressed in terms of harmonic series and cross correlated with the template pulse profile. The pulse phase offsets can be found of a Taylor expansion,

$$\delta\phi = \delta\phi_0 + \delta\nu(t - t_0) + \frac{1}{2}\dot{\nu}(t - t_0)^2, \tag{1}$$

where $\delta\phi$ is the pulse phase offset deduced from the pulse timing analysis, t_0 is the midtime of the observation, ϕ_0 is the phase offset at t_0, $\delta\nu$ is the deviation from the mean pulse frequency (or additive correction to the pulse frequency), and $\dot{\nu}$ is the pulsar's pulse frequency derivative. We fitted the phase offsets to the Taylor expansion. From the fit, we found the pulse period corresponding to the XMM observation as 354.7940 ± 0.0008s and 57.5 days average spin-up rate as $(7.4 \pm 0.9) \times 10^{-13}$ Hz s^{-1}. We did not see any significiant timing noise in the residuals of arrival times, which indicated that the spin up rate was stable through the observations. The average 3-20 keV flux of RXTE observations was $(5.5 \mp 0.5) \times 10^{-10}$ergs^{-1}cm^{-2}. The mean spin-up rate and the average X-ray flux were found to be consistent with the previously observed spin-up rate and X-ray flux correlations during the 1999 outburst (see Fig. 7 in Baykal et al. 2002). Detailed timing noise of RXTE observations is in progress and is not the scope of this paper (Baykal et al. 2004).

In Figure 1, we presented energy dependent pulse profiles of XMM-EPIC PN data. The feature peaking at the phase ~ 0.25 before the peak of the main pulse was a prominent feature of the pulse profile. The pulse fraction was $(50.9 \mp 0.3)\%$ at 0.9-11 keV, whereas it was found to be slightly variable in the energy intervals shown in Figure 1 with a minimum of $(48.5 \mp 0.8)\%$ at 7.5-11 keV and a maximum of $(53.6 \mp 0.7)\%$ at 2.5-5.0 keV.

3.2. Transient 22.7 sec QPO

In the power spectra of the 0.9-11 keV EPIC-PN lightcurve we found quasi periodic oscillations around 0.044 Hz (see Fig. 2). In order to test the significance of these oscillations, we averaged 9 power spectra and rebinned the frequencies by a factor 8. Then we modeled the continuum power spectrum with a broken power law model with the break value $(4.45 \mp 0.16) \times 10^{-2}$ Hz, and the power indices -0.34 ∓ 0.08 and -2.14 ∓ 0.05. We modeled the transient oscillations with a Lorentzian centered at $(4.40 \mp 0.12) \times 10^{-2}$ Hz, with the full width half maximum (FWHM) of $(6.1 \mp 2.0) \times 10^{-3}$ Hz.

To test the significance of this QPO feature, we normalized the power spectrum by dividing it by the continuum and we multiplied this result by 2 (van der Klis 1989). The resultant power spectrum would be consistent with a Poisson distribution for a degree of freedom $2 \times 8 \times 9 = 144$. As seen from the lower panel of Figure 2, there is a prominent peak at ~ 0.044 Hz with a minimum of excess power (including the error of power) 3.62 giving the total power as $3.62 \times 8 \times 9 = 260.64$. This gives the probability of detecting a false signal $Q(260.64|144) = 9.39 \times 10^{-9}$. Since we have 512 frequencies in each power spectra, total probability of having false signal becomes $9 \times 512 \times 9.39 \times 10^{-9} = 4.3 \times 10^{-5}$. Therefore significance of transient oscillations is $1 - 4.3 \times 10^{-5} \simeq 0.99996$ which is consistent with more than 6 sigma level detection. The rms fractional amplitude associated with this QPO feature was found to be $(6.6 \mp 1.9)\%$.

We searched transient oscillations using the RXTE-PCA lightcurves in the 3-20 keV energy range, however we did not see any significant transient oscillations. Then we extracted a $\sim 50\%$ portion of the overall XMM-EPIC PN lightcurve at the 3-10 keV energy range that coincided exactly with the ~ 4.5 ksec part of the RXTE PCA lightcurve on January 6, 2003 and performed power spectral analysis. We found that the significances of 0.044 Hz oscillations for RXTE and XMM lightcurves are 2.5σ and 2.8σ respectively. We concluded that the QPO feature was originated mostly from the soft component of the spectrum or highly transient. Future observations are required to confirm these oscillations.

3.3. Spectral Analysis

We fitted overall background subtracted 1-10 keV spectra of PN, MOS1 and MOS2 to an absorbed power law model (Morrison & McCammon, 1983) with high energy cut-off (White, Swank, Holt 1983). In addition, an iron line feature at 6.42 keV was required in the spectral model (Case 1 in Table 1). However, this model did not fit the spectrum of the source well, giving a reduced χ^2 of 2.69. Adding an additional blackbody component to the

model decreased the reduced χ^2 to 1.23 (Case 2 in Table 1). Joint fit including the PCA data on January 6, 2003 and adding 2% systematic errors (see Wilms et al. 1999; Coburn et al. 2000), was possible to this model with a reduced χ^2 of 1.1 (Case 3 in Table 1 and Figure 3). Using Case 3 (i.e. the joint fit to the model including blackbody component), 1-20 keV unabsorbed flux was found to be 6.6×10^{-10} ergs s^{-1} cm^{-2}. Assuming a source distance of 3.2 kpc (Baykal et al. 2002), this value corresponds to a luminosity of 7.5×10^{35} ergs s^{-1}. To compare with the average X-ray flux, we found 3-20 keV flux of the January 6 observation to be 6.1×10^{-10} ergs s^{-1} cm^{-2}. This value is approximately 10% greater than the 57.5 days average 3-20 keV RXTE-PCA flux. This is reasonable since the XMM observation took place 3.55 days after the periastron passage where the X-ray flux reaches approximately its maximum (see Fig. 5 and 8 of Baykal et al. 2000b). It should be noted that line parameters obtained from 3-20 keV RXTE PCA data agree with those obtained from XMM EPIC data. However exclusion of the blackbody component, while fitting RXTE PCA data only, increases the absorption column density and equivalent width of line emission and make the power law index harder as shown in Table 1, case 4.

To study the spin-phase-resolved spectra using EPIC-PN data, we divided the spin phase into 10 bins, and fitted 1-10 keV spectrum of each bin with the model including blackbody component (i.e. model in case 3). Figure 4 is a plot of the spectral parameters as a function of the spin phase. For all the spin phases, we found that the model gives an iron line peak energy consistent with 6.42 ± 0.04 keV within 1σ, so we chose to fix this parameter. We also checked the consistency of freezing the cut-off energy, iron line sigma, and e-folding energy parameters, and found that these parameters did not vary significantly when they were thawed. From Figure 4, strong modulation (with a factor of ~ 10) of the blackbody flux with the spin phase is evident. Similarly, the flux of the power law component was shown to be varying with the spin phase, but the variation was more moderate (with a factor of ~ 3) than the that of the blackbody component. The iron line feature at 6.42 keV was stronger for the off-pulse phases where the X-ray flux was lower.

4. Discussion and Conclusion

4.1. QPO Feature of SAX J2103.5+4545

Quasi-periodic oscillations in the X-ray band having periods in the range of $\sim 2.5 - 100$s have been observed in many accretion powered X-ray pulsars: 4U 0115+63 (Soong & Swank 1989), EXO 2030+375 (Angelini, Stella,& Parmar 1989), 4U 1626-67 (Shinoda et al. 1990), SMC X-1 (Angelini, Stella,& White 1991), Cen X-3 (Takeshima et al. 1991), V0332+53 (Takeshima et al. 1994), A0535+262 (Finger, Wilson,& Harmon 1996), GRO

J1744-28 (Zhang, Morgan,& Jahoda 1996; Kommers et al. 1997), X Per (Takeshima 1997), 4U 1907+09 (in't Zand, Baykal, & Strohmayer 1998; Mukerjee et al. 2001), XTE J1858+034 (Paul & Rao 1998), LMC X-4, and Her X-1 (Moon & Eikenberry 2001a,b). The QPO feature that we found in the XMM-Newton EPIC-PN light curve of SAX J2103.5+4545 which has a peak period of 22.7 ∓ 0.6s and fractional rms amplitude of 6.6 ± 1.9 percent is quite typical (e.g. In't Zand et. al. 1998; Paul & Rao 1998; Takeshima et al. 1994).

Models that explain the QPO phenomenon in accretion powered X-ray pulsars fall basically into three categories: In the Keplerian frequency model, QPOs are produced due to some inhomogenuities at the inner edge of the Keplerian disk (r_0) and modulate the light curve at the Keplerian frequency $\nu_{QPO} = \nu_K$ (van der Klis et al. 1987). In the beat frequency model, the accretion flow onto the neutron star is modulated at the beat frequency between the Keplerian frequency at the inner edge of the accretion disk and the neutron star spin frequency $\nu_{QPO} = \nu_K - \nu_s$ (Alpar & Shaham 1985). The third model involves accretion flow instabilities (Fronter, Lamb,& Miller 1989; Lamb 1988), and applies only to the sources that have luminosities close to Eddington limit, therefore it should not be applicable to our case for which the luminosity is well below the Eddington limit.

In our case, QPO frequency $\nu_{QPO} = 4.4 \times 10^{-2}$Hz is about one order of magnitude greater than the spin frequency $\nu_s = 2.8185 \times 10^{-3}$ Hz. Therefore, it is difficult to distinguish between a Keplerian model and a beat frequency model.

Assuming that the 22.7 s oscillation in SAX J2103.5+4545 is related to Keplerian orbital motion via either Keplerian frequency model or beat frequency model, and using the QPO and its FWHM values we obtain the radius of inner disk as

$$r_0 = \left(\frac{GM}{4\pi^2}\right)^{1/3} \nu_k^{-2/3} = (1.32^{+0.13}_{-0.11}) \times 10^9 \text{cm}, \tag{2}$$

where M is 1.4 $M_\odot$ for a neutron star and G is the gravitational constant.

From the strong correlation between pulse frequency derivatives and X-ray flux, Baykal et al. (2002) obtained for the distance to the source 3.2 ± 0.8 kpc and for the magnetic field $(12 \pm 3) \times 10^{12}$ Gauss. Using the distance and magnetic field values, the inner edge of the Keplerian disk r_0 can be found as (Ghosh & Lamb 1979)

$$r_0 \simeq 0.52\mu^{4/7}(2GM)^{-1/7}\dot{M}^{-2/7} = (1.67^{+0.23}_{-0.25}) \times 10^9 \text{cm}, \tag{3}$$

where $\mu = BR^3$ is the neutron star magnetic moment with B the equatorial magnetic field, R the neutron star radius, and $\dot{M}$ the mass accretion rate having the value of $\simeq 4 \times 10^{15}$g s^{-1} for an accretion luminosity of $\simeq 7.5 \times 10^{35}$ erg s^{-1} (as estimated in Section 3.3).

The radius of the inner disk inferred from the Keplerian orbital motion of inhomogeneuities and the one inferred from the Ghosh Lamb disk accretion model agree each other. This shows that the idea that the QPOs are formed due to the Keplerian motion of inhomogenuities is indeed promising as the explanation of the QPO of SAX J2103.5+4545 and the observed QPO frequency is consistent with the distance and the magnetic field values estimated by Baykal et al. (2002).

4.2.   Blackbody and Iron Line Features of the Energy Spectrum

XMM-Newton observations of SAX J2103.5+4545 revealed for the first time that the energy spectrum of the source has a blackbody component peaking at ~ 1.90keV with the emission radius of ~ 0.3km. The blackbody radiation may come from the polar cap of the neutron star as it appears to for the Be/X-ray pulsar system EXO 2030+375 (Reig & Coe 1999; Sun et al. 1994) and the millisecond X-ray pulsars SAX J1808.4-3658 (Gierlinski, Done,& Didier 2002) and XTE J0920-314 (Juett et al. 2003). Blackbody emission radii on these X-ray pulsars are reported to be greater than ~ 1km. The relatively high surface magnetic field of SAX J2103.5+4545 ($\sim 10^{13}$ Gauss) is probably the reason for the relatively small blackbody emission radius (~ 0.3 km) compared to these X-ray pulsars. Although the contribution of blackbody component is relatively more significant for lower energies (i.e. energies smaller than ~ 3 keV), power law flux is ~ 3 times greater than the blackbody flux even at the 1-3 keV energy band.

In our case, it is unlikely that the blackbody emission comes from the reprocessed emission of the surrounding material or the accretion disk as in the case of Her X-1 (Endo et al. 2000), Cen X-3 (Burderi et al. 2000), SMC X-1 and LMC X-4 (Paul et al. 2002), since blackbody component in such cases is expected to be softer ($kT \sim 0.1$keV). Lower blackbody temperature and smaller blackbody emission radius at the off-pulse phase shown in Figure 4 are also indications of the plausibility of the polar cap emission interpretation, as the regions of the soft polar cap emission must align with the peak of the X-ray pulse of the pulsar.

Using the spin-phase resolved spectroscopy, strength of the iron line feature at ~ 6.42keV was also found to vary significantly with the spin phase as seen in Figure 4. The peak energy of this feature clearly shows that it corresponds to the fluorescent iron K-line complex. This line complex feature is observed in the spectra of most of the X-ray pulsars (White et al. 1983; Nagase 1989) and is generally thought to be produced by the ions less ionized than Fe XVIII in a relatively cool matter around the neutron star (e.g. accretion disk, accretion disk corona) by fluorescent Kα transition.

Variation of the iron line feature with the spin phase can then be interpreted as a sign that it is mainly produced outside the polar cap region of the neutron star, thus should have a peak at the off-pulse parts of the spin phase. From Figure 4, we see that iron line flux and iron line equivalent width vary strongly with the spin phase, peaking at the off-pulse. Similar pulse phase dependence of the iron line feature is also observed in Her X-1 (Choi et al. 1994).

REFERENCES

Alpar, M.A., Shaham, J. 1985, Nature, 316, 239

Angelini, L., Stella, L., Parmar, A.N. 1989, ApJ, 346, 906

Angelini, L., Stella, L., White, N.E. 1991, ApJ, 371, 332

Baykal, A., Stark, M., Swank J. 2000a, IAU Circ. 7355

Baykal, A., Stark, M., Swank J. 2000b, ApJ, 544, L129

Baykal, A., Stark, M., Swank J. 2002, ApJ, 569, 903

Baykal, A. et al. 2004, in preparation

Burderi, L., Di Salvo, T., Robba, N.R. et al. 2000, ApJ, 530, 429

Choi, C.S., Nagase, F., Makino, F. 1994, ApJ, 437, 449

Coburn, W., Heindl, W.A., Wilms, J. et al. 2000, ApJ, 543, 351

Deeter, J.E., Boynton, P.E., 1985, in Proc. Inuyama Workshop on Timing Studies of X-Ray Sources, ed. S. Hayakawa & F. Nagase (Nagoya: Nagoya Univ.), 29

Endo, T., Nagase, F., Mihara, T. 2000, PASJ, 52, 223

Finger, M.H., Wilson, R.B., Harmon, B.A. 1996, ApJ, 459, 288

Fronter, B., Lamb, F.K., Miller, G.S. 1989, Nature, 342, 775

Ghosh, P., Lamb F.K. 1979, ApJ, 234, 296

Gierlinski, M., Done, C., Didier, B. 2002, MNRAS, 331, 141

Hullemann, F., in't Zand, J.J.M., Heise, J. 1998, ApJ, 337, L25

in't Zand, J.J.M., Baykal, A., Strohmayer, T.E. 1998, ApJ, 496, 386

Jahoda, K., Swank J., Giles A.B. et al. 1996, Proc. SPIE, 2808, 59

Juett, A.M., Galloway, D.K., Chakrabarty, D. 2003, ApJ, 587, 757

Kommers, J.M., Fox, D.W., Lewin, W.H.G. et al. 1997, ApJ, 482, L53

Lamb, F.K. 1988, Adv. Space Res., 8, 421

Lutovinov, A.A., Molkov, S.V., Revnivtsev, M.G. 2003, AstL, 29, 713

Moon, D., Eikenberry, S.S. 2001a, ApJ, 549, L225

Moon, D., Eikenberry, S.S. 2001b, ApJ, 552, L135

Morrison, R., McCammon, D. 1983, ApJ, 270,119

Mukerjee, K., Agrawal, P.C., Paul, B. et al. 2001, ApJ, 548, 368

Nagase, F. 1989, PASJ, 41, 1

Paul, B., Rao, A.R. 1998, A& A, 1998

Paul, B., Nagase, F., Endo, T. et al. 2002, ApJ, 579, 411

Reig, P., Coe, M.J. 1999, MNRAS, 302, 700

Reig, P., Mavromatakis, F. 2003, ATEL, 173

Shinoda, K., Kii, T., Mitsuda, K. 1990, PASJL, 42, 27

Soong, Y., Swank, J. 1989, in Proc. 23d ESLAB Symp., Two Topics in X-ray Astronomy, Vol. 1, ed. N. White (Garching: ESA), 617

Sun, X.-J., Li, T.-P.., Wu, M. et al. 1994, A& A, 289, 127

Struder, L., Briel, U., Dennerl K. et al. 2001, A& AL, 365, 18

Takeshima, T., Dotani, T., Mitsuda, K. et al. 1991, PASJL, 43, 43

Takeshima, T., Dotani, T., Mitsuda, K. et al. 1994, ApJ, 436, 871

Takeshima, T. 1997, BAAS, 19111104

Turner, M.J.L., Abbey, A., Arnaud, M. et al. 2001, A& AL, 365, 27

van der Klis, M., Stella, L., White, N. et al. 1987, ApJ, 316, 411

van der Klis, M. 1989, in Proc. NATO-ASI on Timing Neutron Stars, ed. H.Ögelman and
    E.P.J. van den Heuvel (Dordrecht:Kluwer), 27

White, N.E, Swank, J.H., Holt, S.S. 1983, ApJ, 270,711

Wilms, J., Nowak, M.A., Dove, J.B. et al. 1999, ApJ, 522, 460

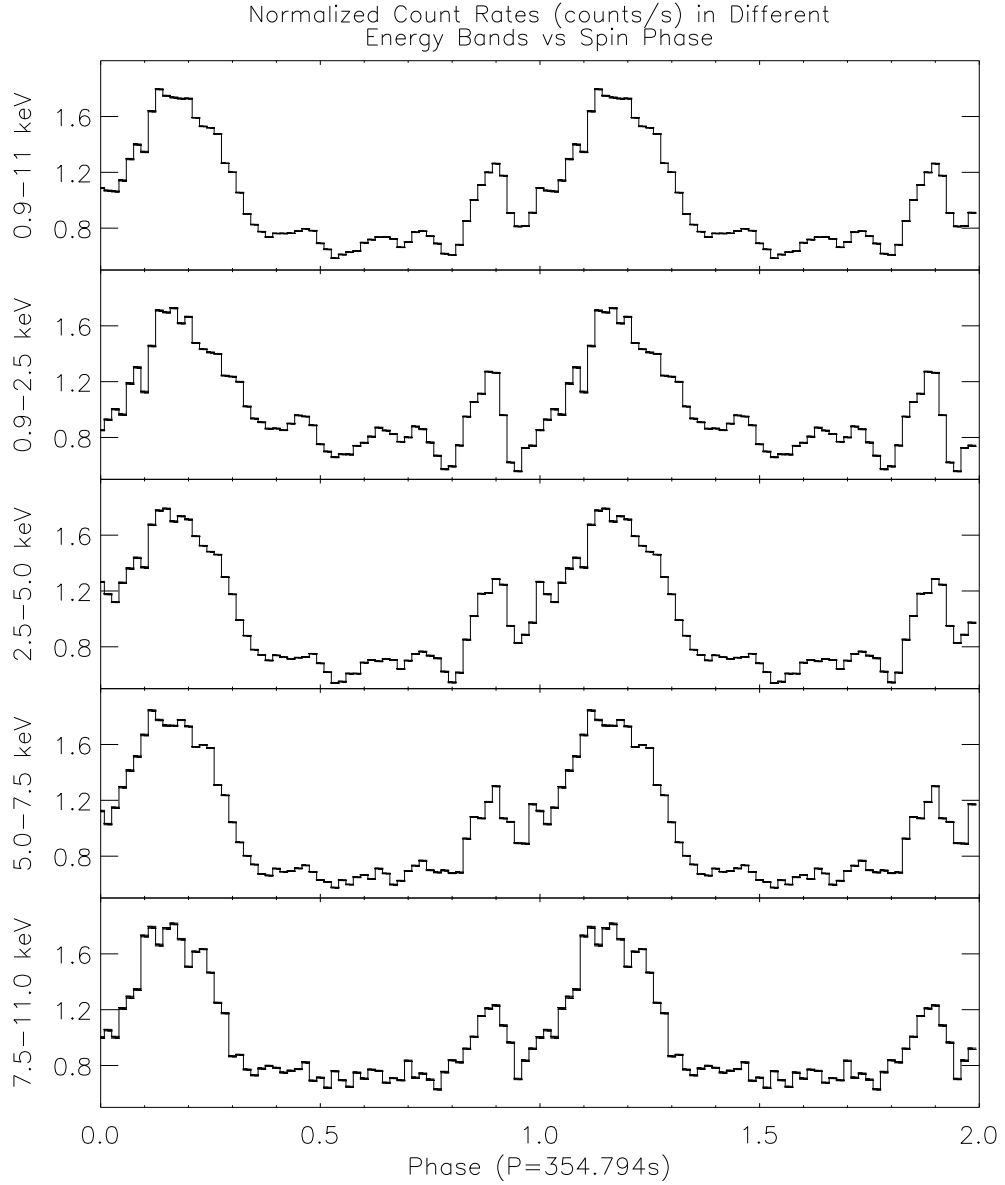Zhang, W., Morgan, E.H., Jahoda, K. 1996, ApJ, 469, L29

Fig. 1.— Energy dependence of the pulse profiles of SAX J2103.5+4545. Pulse profiles were found by using EPIC-PN lightcurves that cover the energy ranges from top to bottom respectively.
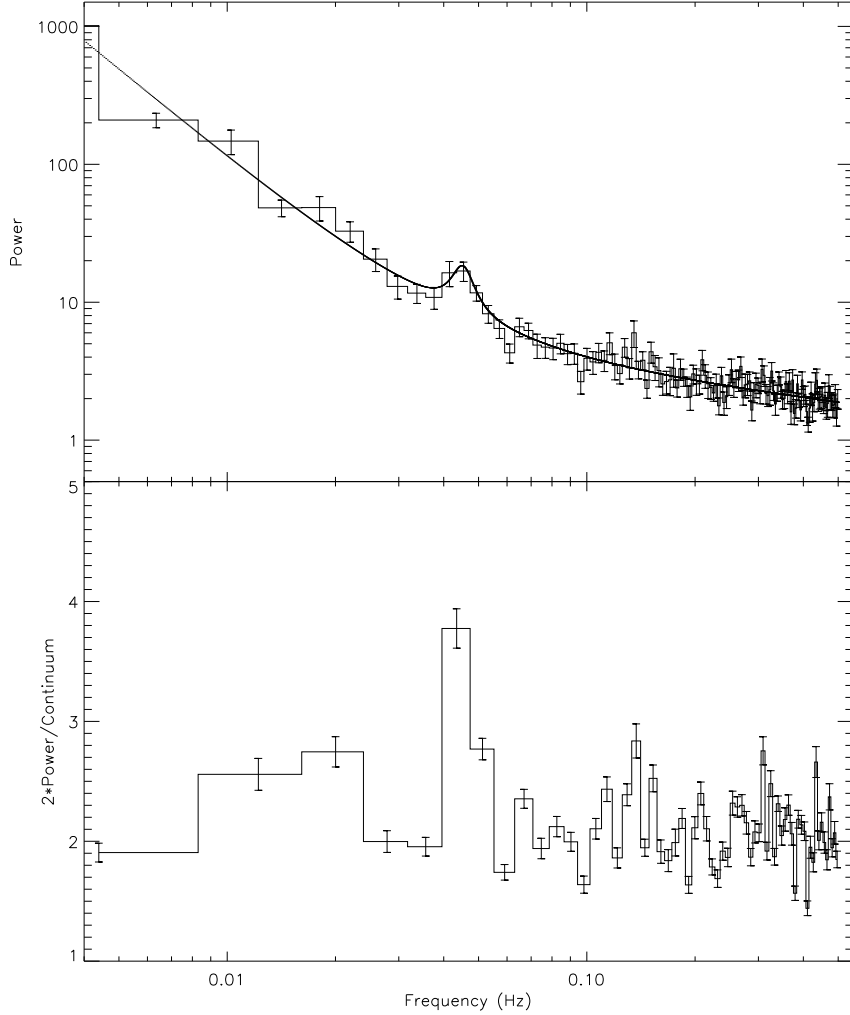
Fig. 2.— **(top)** Power spectrum obtained from the 0.9-11.0 keV EPIC-PN lightcurve and rebinned by a factor of 4. QPO feature centered at 0.044 Hz is the prominent feature of the power spectrum. **(bottom)** Power spectrum rebinned by a factor of 8, multiplied by 2, and divided by the continuum fit consisting of a broken power law model with the power indices -0.34 ∓ 0.08 and -2.14 ∓ 0.05. Applying the method discussed by van der Klis (1989), significance of the QPO feature was calculated to be more than 6σ confidence level using the value of the peak at ~ 0.044 Hz as shown in this plot.
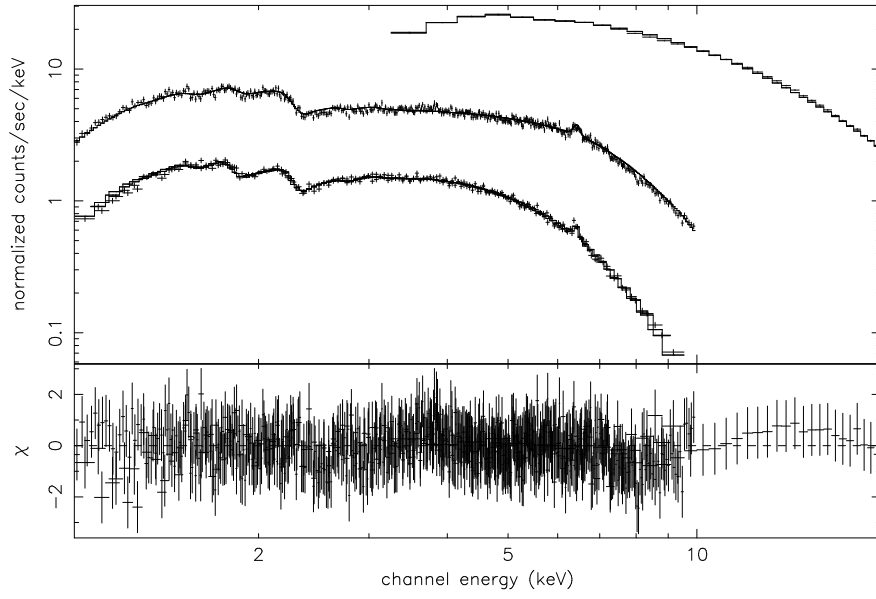
Fig. 3.— 1-20 keV combined PN, MOS1, MOS2 and PCA spectrum of SAX J2103.5+4545 observed on January 6, 2003. The bottom panel shows the residuals of the fit in terms of σ values.
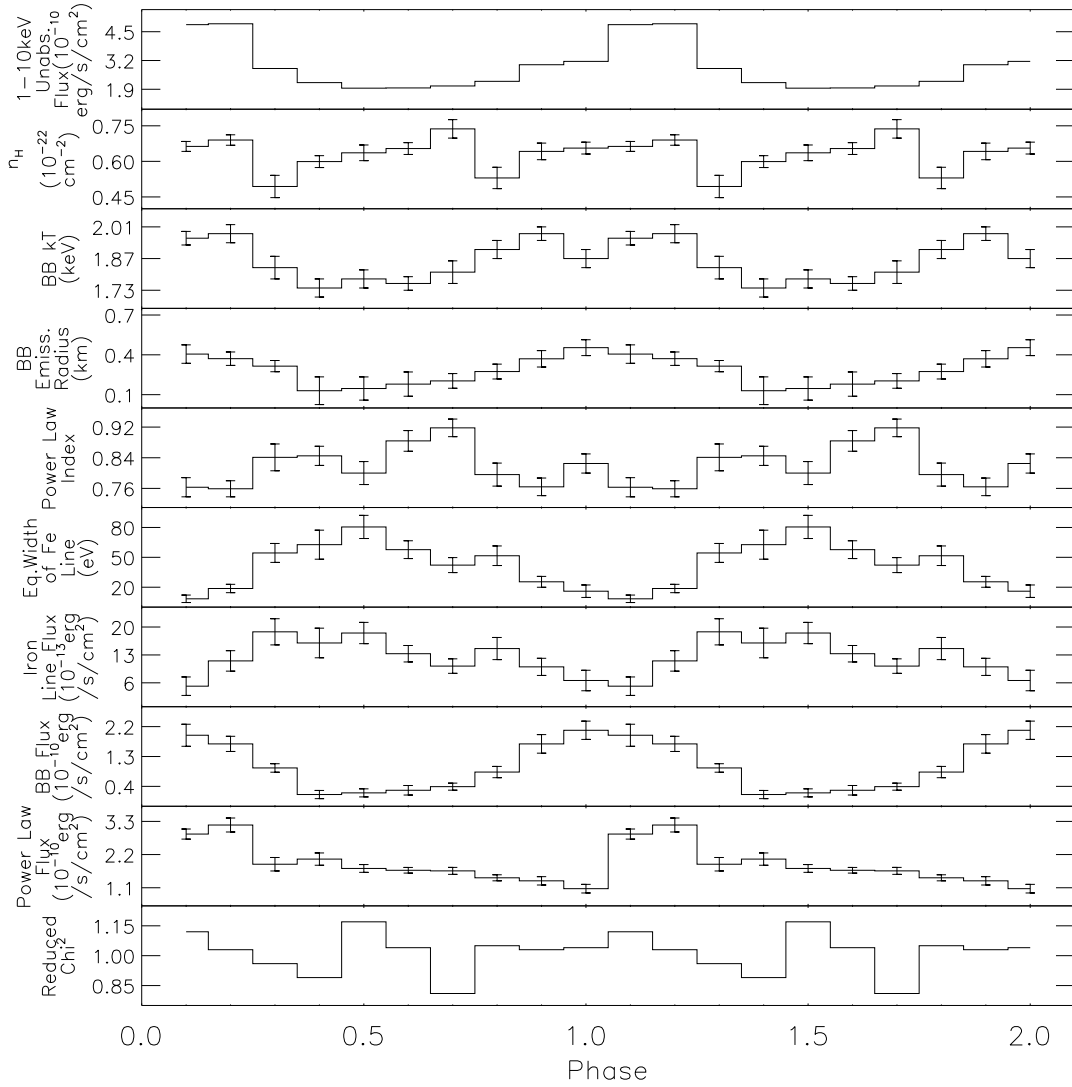
Fig. 4.— Spin phase dependence of 1-10 keV X-ray flux in units of 10^{-10} ergs s^{-1} cm^{-2}, Hydrogen column density in units of 10^{22} cm^{-2}, blackbody kT in units of keV, emission radius of the blackbody (assuming a source distance of 3.2 kpc) in units of km, photon index of the power law component of the spectral model, equivalent width of the iron line in units of eV, flux of the iron line in units of 10^{-13} ergs s^{-1} cm^{-2}, blackbody flux in units of 10^{-10} ergs s^{-1} cm^{-2}, power law flux in units of 10^{-10} ergs s^{-1} cm^{-2}, and reduced χ^2. All of the errors show 1σ confidence level. The spectral model used in fitting consists of an absorbed power law model with high energy cut-off, a soft blackbody component and an Iron line feature modeled as a Gaussian. The values of iron line peak energy, iron line sigma, cut-off and e-folding energies were found to be consistent with the constant values 6.42 keV, 0, 7.89 keV, and 27.1 keV respectively for all the spin phases, so these values were kept fixed while the values of the other model parameters were found.

Table 1: Spectral Models of SAX J2103.5+4545

Parameter	Case 1 (without BB) (PN,MOS1,MOS2)	Case 2 (with BB) (PN,MOS1,MOS2)	Case 3 (with BB) (PN,MOS1,MOS2,PCA)	Case 4 (without BB) (PCA)
Multiplication Factors[1] (1.00 for EPIC-PN)				
——MOS 1	0.77 ∓ 0.01	0.76 ∓ 0.01	0.76 ∓ 0.01	na
——MOS 2	0.76 ∓ 0.01	0.75 ∓ 0.01	0.75 ∓ 0.01	na
——PCA	na	na	1.26 ∓ 0.01	na
n_H (10^{22}cm^{-2})	0.90 ∓ 0.02	0.68 ∓ 0.01	0.66 ∓ 0.02	2.98 ∓ 0.14
Iron Line Energy (keV)	6.41 ∓ 0.04	6.42 ∓ 0.02	6.42 ∓ 0.02	6.36 ∓ 0.06
Iron Line Sigma (keV)	0 (fixed)	0 (fixed)	0 (fixed)	0.68 ∓ 0.13
Iron Line Equivalent Width (eV)	48.0 ∓ 7.0	37.1 ∓ 5.3	36.5 ∓ 5.0	107 ∓ 15
Iron Line Flux (ergs s^{-1} cm^{-2})	$(1.69 \mp 0.24) \times 10^{-12}$	$(1.37 \mp 0.20) \times 10^{-12}$	$(1.36 \mp 0.19) \times 10^{-12}$	$(5.14 \mp 0.72) \times 10^{-12}$
Iron Line Normalization (photons cm^{-2} s^{-1})	$(1.65 \mp 0.24) \times 10^{-4}$	$(1.33 \mp 0.19) \times 10^{-4}$	$(1.32 \mp 0.18) \times 10^{-4}$	$(5.00 \mp 0.70) \times 10^{-4}$
Blackbody kT (keV)	na	1.91 ∓ 0.04	1.88 ∓ 0.02	na
Blackbody Normalization (km^2 (10kpc)$^{-2}$)	na	0.88 ∓ 0.04	0.83 ∓ 0.07	na
Power Law Index	0.83 ∓ 0.02	0.82 ∓ 0.04	0.77 ∓ 0.05	1.14 ∓ 0.05
Power Law Normalization (photons keV^{-1} cm^{-2} s^{-1})	$(1.61 \mp 0.32) \times 10^{-2}$	$(1.03 \mp 0.26) \times 10^{-2}$	$(1.01 \mp 0.27) \times 10^{-2}$	$(3.88 \mp 0.07) \times 10^{-2}$
Cut-off Energy (keV)	7.89 (fixed)	7.89 (fixed)	7.89 (fixed)	7.89 (fixed)
E-folding Energy (keV)	27.1 (fixed)	27.1 (fixed)	27.1 (fixed)	27.1 (fixed)
Reduced χ^2	2.69 (1259 d.o.f)	1.23 (1253 d.o.f)	1.11 (1283 d.o.f)	1.20 (30 d.o.f)

[1] For the cases 1, 2 and 3, we multiplied the entire model with a factor which is varying with the instrument to account for the different normalizations of the instruments (the value of the constant was fixed to be 1 for EPIC-PN).